University of California, Merced

Pressure vessel design for use in miscibility testing

by

Brian Martin-Gutierrez

Submitted in Partial Fulfillment of the

Requirements for the Degree of

Master of Science in Mechanical Engineering

Committee:

Ashlie Martini (Advisor)
Venkattraman Ayyaswamy
Reza Ehsani

Department of Mechanical Engineering
School of Engineering

2022

The Thesis of Brian Martin-Gutierrez is approved:

_____

Ashlie Martini, Advisor Date

_____

Reza Ehsani Date

_____

Venkattraman Ayyaswamy Date

University of California, Merced

Acknowledgments

I am deeply indebted to Professor Ashlie Martini for her invaluable guidance, support, and patience. I would also like to thank the members of the Martini Research Group for their help throughout my academic and research endeavors.

Abstract

Knowledge of lubricant and refrigerant miscibility is necessary for the optimal design and function of compressors in refrigeration systems. Without adequate knowledge of mixture miscibility, compressor lubricants can drift into refrigerant systems, fail to return to the compressor and cause build-up in the pipes. This entrapped lubricant will reduce the systems efficiency by lowering the heat transfer coefficient of the system and introducing flow irregularities. To obtain data on refrigerant and lubricant miscibility a pressure vessel needed to be designed and manufactured. This pressure vessel needed to withstand a working pressure of 150 bar, a temperature range of -40 C to 160 C, and have an integrated mixer. ASME, ISO, and ASHRAE standards were referenced in the design of this vessel to ensure proper function and safety. Stress and displacement simulations were conducted using SolidWorks to help inform the final design. Additionally, ANSYS and COMSOL were leveraged for fluid mixing simulations to determine optimal mixing impeller design for our system. The rushton and hydrofoil impellers showed

the greatest eddy diffusivity and mixing potential. Overall, this work has produced a functioning pressure vessel, a system for temperature regulation of the pressure vessel, and a proposed method to obtain lubricant and refrigerant miscibility data.

Contents

List of Tables

List of Figures

1. Introduction

1.1 Background and Motivation

1.1.1 Miscibility

Understanding the physical properties of refrigerant-lubricant mixtures is obligatory for the design of future refrigeration systems and circuits. Without adequate knowledge of mixture miscibility, compressor lubricants can drift into refrigerant systems, fail to return to their necessary destination and cause build-up in the pipes, visualised in Fig. 1.1. If the lubricant fails to return to the compressor, the system can become starved of lubricants and lead to premature system failure [20, 16, 33, 2]. In addition to eventual failure, if lubricant remains in the refrigeration loop, the systems overall efficiency will decrease because the lubricant has a much lower heat transfer coefficient than the refrigerant.

The process to determine miscibility varies greatly on the lubricants and refrigerants to be tested. While most data on miscibility is sparse due to the competitive nature of the industry, there are a few common testing methods. First, experimental

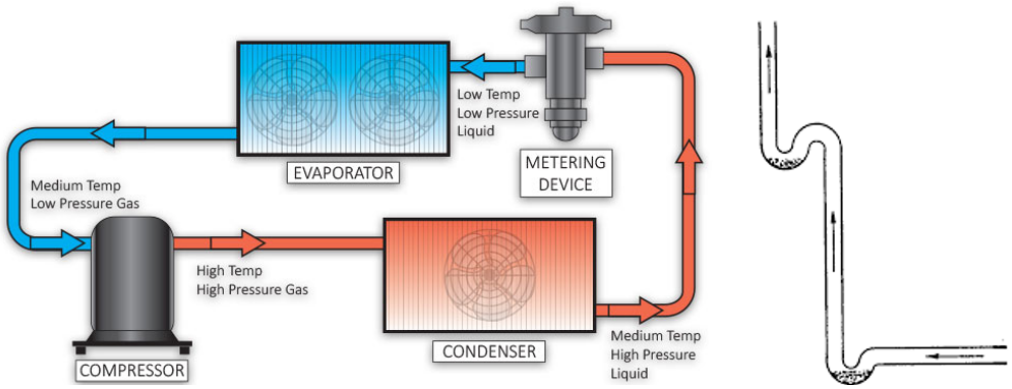

Figure 1.1: Example of basic refrigeration system [left] and pipe with lubricant accumulation [right] [3]

analysis with slim tubes at low pressures [39, 6]. These tests are typically conducted using transparent quartz tubes which can withstand pressures of up to 35 bar and temperatures from -70 °C to 40 °C. Second, experimental analysis with custom pressure vessels from low to medium pressures [30, 20, 31, 18]. The pressure range for custom made vessels is dependent on the design specs, but typical tests are ran at pressures up to 69 bar. Temperature ranges for these test also vary greatly but can reach from -40 °C up to 130 °C. Aside from the apparatus used to contain the refrigerant and lubricant mixture, the remaining components of the system are usually similar. They include a thermostatic bath for temperature regulation, temperature and pressure transducers, multiple valves, and data acquisition system.

Regardless of the system employed, all results were analyzed visually. Fig. 1.2 demonstrates the visual results of a miscible mixture (a) and non miscible mixtures (b,c).

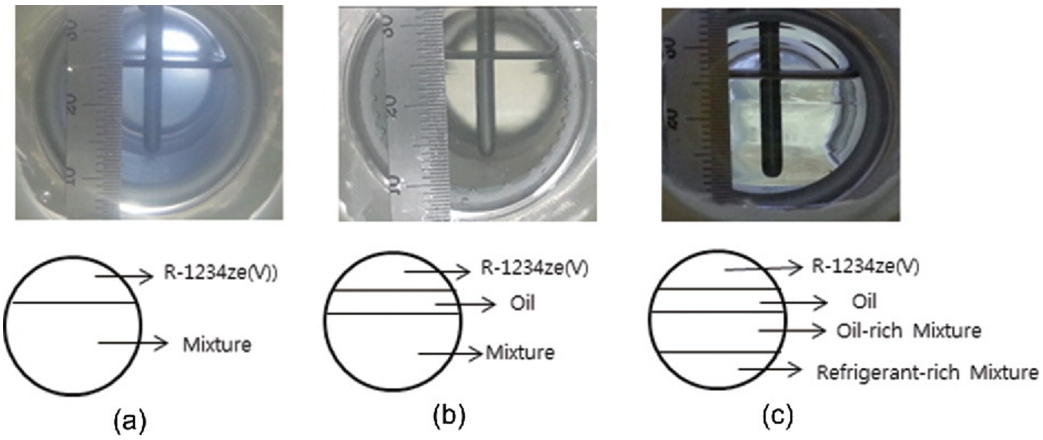

Figure 1.2: Visual example of miscible and non-miscible mixtures [30]

1.1.2 Lubricants

Lubrication is vital to the performance, reliability, and energy efficiency of mechanical systems [14]. Depending on the mechanical systems needs, the lubricant composition can vary drastically. Consideration for the necessary lubricant properties must be part of the mechanical system design process or else problems with wear and reliability will arise [23]. For instance, aerospace applications subject to extreme temperature and vacuum conditions may be more aptly suited for solid lubricants rather than liquid lubricants [37]. Negligence of the lubricant choice in the design phase can lead to the failure and loss of expensive systems [9]. For systems subject to less harsh environments, solid,liquid and gaseous lubricants can be used alone or in tandem with each other to reduce friction and wear [29].

Refrigeration systems also have a need for lubricants, namely liquid lubricants. Fig. 1.1 shows a simplified refrigeration system and one of the main components of that system is a compressor. The function of the compressor in this system is

to pressurize incoming gas by reducing its volume, thus allowing it to continue flowing through the system. In most cases, compressors used for refrigeration systems need to be hermetically sealed to avoid refrigerant leaks. This means there is a higher chance for the oil lubricating the compressor's motor to migrate into the refrigeration line.

Over the years, the main oils used in refrigeration heating and cooling (RHAC) systems have included; mineral oil (MO), polyol ester oil (POE), and alkyl benzne oil (AB) [39]. MOs are among the most ubiquitous in RHAC systems due to their cost effectiveness and miscibility with most CFCs and HCFCs [40]. Unfortunately, as the pressures and temperatures required for new refrigerants to operate increase, traditional lubricant formulations will not suffice.

1.1.3 Refrigerants

Since the inception of mechanical air conditioning and refrigeration, the main focus placed on refrigerants has been about performance. Throughout the late 1800's and up until the mid-1900's, commonly used refrigerants included Sulphur Dioxide, Carbon Dioxide, Ammonia, Methyl Chloride, and Hydrocarbons [20]. Many of these refrigerants had the pitfall of being toxic and flammable [36]. As commercial refrigeration systems became more prevalent, concerns of public safety began to rise. To address these concerns, synthetic refrigerants like ChloroFluoroCarbon (CFC) and HydroChloroFluoroCarbons (HCFC) were developed [20]. Commercialization of these products ushered in the second generation of refrigerants.

As knowledge and acceptance of climate change progressed, it became apparent the refrigerants which ameliorated early concerns of toxicity and flammability, had a significant contribution to ozone depletion. From the mid to late 1990's there was another shift in the refrigerant market, this time towards refrigerants with lower Ozone Depletion Potential (ODP) and Global Warming Potential (GWP). A key component in ODP is the inclusion of chlorine in refrigerants. It was discovered that one chlorine atom can destroy nearly 100,000 ozone molecules [4]. This potential for harm to the environment led to the international ban on the production of CFC R12, commonly known as Freon, and other refrigerants [1].

Seeking new alternatives, HydroFluoroCarbons [HFC] and HydroFluoroOlefin [HFO] were developed. In addition to the development of new synthetic refrigerants, previously discounted natural refrigerants started to gain favor. Fig. 1.3 shows the difference in ODP and GWP betwen R12 and Carbon Dioxide. We still find ourselves in this current trend of attempting to maximize refrigerant performance, while minimizing adverse effects to the environment.

Refrigerant group	Refrigerant example	ODP	GWP_{100}	Atmospheric lifetime (years)	Flammability
CFCs	R-11, R-12, R-115	0.6–1	4750–14,400	45–1700	Nonflammable
HCFCs	R-22, R-141b, R-124	0.02–0.11	400–1800	1–20	Nonflammable
HFCs	R-407C, R-32, R-134a, R-152a	0	140–11,700	1–300	Nonflammable or mildly flammable
HFOs	R-1234yf, R-1234ze(E), R-1234yz	0	0–12	–	Mildly flammable
Natural refrigerants	CO_2(R-744), NH_3(R-717), HC (Propane (R-290), n-Butane(R-600), iso-Butane (R-600a))	0	0	Few days	HCs: Highly flammable R717: Flammable R744: Nonflammable

Figure 1.3: Summary of historical refrigerants. Adapted from [25]

Natural Refrigerants

The main benefits of natural refrigerants are their zero ODP, low GWP, and solubility with many common MOs. Natural refrigerants also don't contain Chlorine or Florine atoms, preventing them from forming strong acids when coming in contact with water [4]. The three main natural refrigerants are Hydrocarbons (HCs), Ammonia, and Carbon Dioxide (CO2). Unfortunately, each natural refrigerant also comes with a trade off making them non optimal to work with.

Hydrocarbons (HCs) are a group of naturally produced substances, whose most popular members can be seen in Fig. 1.4. Their main drawback is their flammability,

but with appropriate safety measures this danger can be mitigated. Many local and international standards, including ASHRAE 15, focus on the necessary precautions to design and safely operate systems with flammable refrigerants. Two of the main solutions are to limit the amount of the hydrocarbons in the system and require a hermetically sealed system [12]. Per ASHRAE 15, there must also not be any devices which produce open flames or hot surfaces greater then 427 C in any room where refrigeration equipment is installed.

Data	Refrigerants		
	Propane (R290)	***n*-butane (R600)**	**iso-butane (R600a)**
Natural	Yes	Yes	Yes
ODP	0.0	0.0	0.0
GWP, 100 years	3.0	3.0	3.0
Density at 25 °C (kg/m^3)	492.7	532.5	550.7
Flammability limits (vol%)	2.1–11.4	1.7–10.3	1.9–10.0
Molecular mass (kg/kmol)	44.1	58.1	58.1

Figure 1.4: Most popular HCs. Adapted from [8, 13]

Ammonia is another natural refrigerant which has had a resurgence despite its safety concerns. It can most commonly be found in industrial refrigeration systems for food and warehouse cooling [28]. When present in large quantities , such is the case for most warehouse applications, restrictions are placed on the location of the compressor and appropriate gas leak detection systems are required [28]. These

restriction are due to the inherent toxicity of ammonia. With appropriate safety systems, personal can easily be evacuated before prolonged exposure can occur. Another issue which must be addressed in the design phase of the refrigeration system is Ammonia's incompatibility with many elastomers.

CO2 is uniquely positioned among natural refrigerants because it is neither flammable nor toxic [4]. Its drawback come in the form of its operating conditions. Efficient CO2 systems need to operate at much higher pressures than normal, typically up to 150 bar, and they must operate at low temperatures. Optimal performance for CO2 systems occurs bellow its sub-critical temperature of 31.1 $^{\circ}$C [26]. However, if these stringent requirements are met, CO2 systems can be among the most energy efficient and environmentally friendly [19].

1.2 Summary

While companies optimize refrigerants to meet the ever changing safety and environmental standards, there must also be an equal push to optimize the lubricants they are mixed with in refrigeration systems. Since compressors have also continued to evolve over the years, their need for improved lubrication to operate efficiently has increased. Without proper refrigerant lubricant miscibility, the lubricant may fail to completely return to the compressor and cause lubricant starvation of the motor bearings. Additionally, lubricant which fails to return to the compressor may lower the heat transfer rate of the system and introduce flow related issues due to build-up. Refrigerant and lubrication interactions need to be

carefully cataloged to ensure optimal performance and safety of a refrigeration system.

1.3 Overview of Thesis

The contents of this thesis focuses on the research conducted to design and produce a pressure vessel intended for miscibility analysis. The scope of this project had to be narrowed to design for a few key refrigerants and test parameters to reduce complexity and facilitate manufacturing. In chapter 2, the scope and design parameters for the pressure vessel are described in detail. It includes explanations for all the steps and decisions that were made throughout the design process and changes that were made post manufacturing. Additionally, a procedure is proposed for the miscibility test. Chapter 3 includes all the simulations and study's that were conducted to inform the design decisions in the previous chapter. Lastly, Chapter 4 summarizes the presented research and provides suggestions for future work.

2. Design and Methods

2.1 Introduction

Pressure vessels are sealed containers designed to house gasses or liquids at pressures greater than the ambient environment. Due to the hazardous nature of pressurized vessels, their design and manufacturing are closely regulated by the American Society of Mechanical Engineers (ASME). ASME publishes the Boiler Pressure Vessel Codes (BPVC) every other year to ensure that optimal and best practices are being followed. When first designing this pressure vessel, BPVC Section VIII Divisions 1 and 2 were referenced. The goal of this project was to design a pressure vessel capable of housing refrigerant and lubricant mixtures at a working pressure of 150 bar over a wide temperature range to measure miscibility. The vessel had to handle the wide temperature and pressure ranges, while being chemically resistant to natural refrigerants, like ammonia and CO2.

2.2 Vessel Design

2.2.1 Criteria

The pressure vessel was designed with the goal of obtaining data of the miscibility of lubricant and refrigerant mixtures. To achieve this, the pressure vessel needed to allow for the visual inspection of the mixtures under varying temperatures and pressures. It was important to not only design our vessel for the testing of current refrigerants in the market, but also plan for future refrigerants currently in development. To address these concerns, initial design criteria were selected to allow for the testing scope to be expanded in the future. First, since data for miscibility would be obtained via visual inspection, it was necessary for there to be a sight glass which allowed for the observation of the internal mixture. Second, to ensure the lubricant and refrigerant are given the opportunity to homogenize, there needed to be a mixer installed in the vessel to expedite and facilitate this process. Third, to mimic operating conditions of CO2 in industrial applications, the pressure vessel needed to withstand a working pressure of up to 150 bar. Fourth, to ensure accurate testing and data collection, there needed to be a pressure and temperature transducer to relay accurate information of the conditions in the pressure vessel. Lastly, the pressure vessel had to also be able to withstand temperature changes ranging from -40 °C to 160 °C. These were the five main criteria which had to be met in order for this vessel to produce the desired data. With these criteria as a foundation, it will be possible to scale to different types of lubricants and refrigerants as demands change.

2.2.2 Material Selection

In commercial refrigeration systems proper material selection is important because of the thermodynamic and transport properties of the system [32]. For this test rig, material compatibility is important to produce safe, reliable, and reproducible data.

Pressure Vessel

Due to the high pressure we will be working with, the ultimate tensile strength of the material was one of the design drivers. The BPVC has guidance for the maximum allowable stress values (MASV) for common materials used in vessel design. Fig. 2.1 shows the MASV adapted from the tables in BPVC Section Viii division 1 and 2. The differences in MASV between division 1 and 2 are due to the different safety factors required by each method, 3.5 and 2.5 respectively.

While in most cases the MASV is greater for carbon steels, it is paramount the vessel be resistant to corrosion and degradation from refrigerants. Because of this, high alloy steels were preferred over carbon steels. While regular 316 Stainless Steel (316 SS) is common in most industrial refrigeration applications, 316L Stainless Steel (316L SS) was chosen due to its lower carbon content [21]. This would allow for a greater variety of refrigerants to be used in the future with less danger of corrosion. Another benefit of the lower carbon content in 316L SS is it's superiority for welding.

Maximum Allowable Stress Value for Common Steels				
Material	**Spec. Nbr**	**Grade**	**DIVISION 1** -20°F to 650°F	**DIVISION 2** -20°F to 650°F
Carbon Steel Plates and Sheets	SA - 516	Grade 55	13,800	18,300
		Grade 60	15,000	20,000
		Grade 65	16,300	21,700
		Grade 70	17,500	23,300
	SA - 285	Grade A	11,300	15,000
		Grade B	12,500	16,700
		Grade C	13,800	18,300
	SA - 36		12,700	16,900
	SA - 203	Grade A	16,300	21,700
		Grade B	17,500	23,300
		Grade D	16,300	21,700
		Grade E	17,500	23,300
High Alloy Steel Plates	SA - 240	Grade 304	11,200	20,000
		Grade 304L	-	16,700
		Grade 316	12,300	20,000
		Grade 316L	10,200	16,700

Figure 2.1: Maximum allowable stress values for common steels

Gaskets

There are many concerns when choosing the appropriate gasket for refrigerant systems: swelling of material, change in mechanical properties, flammability, and permeation [17]. Although various refrigerants will be used in this pressure vessel, the two main refrigerants of focus were R717 (Ammonia) and R744 (carbon dioxide). These were referenced for design purposes. Referencing Fig. 2.2, it was determined that Polytetrafluoroethylene (PTFE) was the most suitable material to use since it didn't suffer from permeation or swelling like the elastomer gasket candidates. PTFE is also able to handle temperatures from -40 °C to 280 °C, far

greater than typical elastomers [22]. Furthermore, expanded PTFE (ePTFE) was chosen over traditional PTFE because it is more suitable for handling compressive loads [15]. This is due to ePTFE having a porous internal micro-structure, a result of its manufacturing process, which allows it to reduce constant creep under extended periods of compression [15].

				Plastics material					Elastomer material		
N°	Name	Formula	R #	PTFE	PCTFE	PVDF	PA	PP	IIR	NBR	CR
1	ACETYLENE	C_2H_2		A	A	A	$A_{W,I}$	A	A	$NR_{W,I}$	$NR_{W,I}$
2	AMMONIA	NH_3		A	A	$NR_{G,W}$	A	A	A	A_W	?
3	ARGON	Ar		A	A	A	A	A	A	A	A
4	ARSINE	AsH_3		A	A	A	A	?	A	A	A
5	BORON TRICHLORIDE	BCl_3		A	A	A	NR_W	A	NR_W	NR_W	NR_W
6	BORON TRIFLUORIDE	BF_3		A	A	A	NR_W	A	NR	NR_W	NR_W
7	BROMOCHLORODIFLUOROMETHANE	$CBrClF_2$	R12B1	A	A_S	A	A	A	?	NR_S	A
8	BROMOTRIFLUOROMETHANE	$CBrF_3$	R13B1	A	A_S	?	A	$A_{S,W}$	A_S	A_S	A_S
9	BROMOTRIFLUOROETHYLENE	C_2BrF_3	R123B1	A	A_S	?	?	?	?	?	?
10	BUTADIENE (1,2)	C_4H_6		A	A	A	A	A	$NR_{S,M}$	$NR_{S,M}$	$NR_{S,M}$
11	BUTADIENE (1,3)	C_4H_6		A	A	A	A	A	$NR_{S,M}$	$NR_{S,M}$	$NR_{S,M}$
12	BUTANE	C_4H_{10}		A	A	A	A	A	NR_S	A	A
13	BUTENE	C_4H_8		A	A	A	A	A	$NR_{S,M}$	A	NR_S
14	BUTENE cis	C_4H_8		A	A	A	A	A	$NR_{S,M}$	A	NR_S
15	BUTENE trans	C_4H_8		A	A	A	A	A	$NR_{S,M}$	A	NR_S
16	CARBON DIOXIDE	CO_2		A	A	A	A	A	NR_S	$NR_{S,W}$	$NR_{S,W}$
17	CARBON MONOXIDE	CO		A	A	A	A	A	A_G	A	A
18	TETRAFLUOROMETHANE	CF_4	R14	A	$A_{S,W}$	A	A	A	A	A	A
19	CARBONYL SULPHIDE	COS		A	A	A	A	?	NR_W	NR_W	NR_W
20	CHLORINE	Cl_2		see 6.2.1.2 Warning : There is a risk of violent reactions							
20	CHLORINE	Cl_2		A	A	A	NR_F	NR_F	NR_F	NR_F	NR_F
21	CHLORODIFLUOROMETHANE	$CHClF_2$	R22	A_P	A_S	?	A	A_P	A_S	NR_S	A_S

A = Acceptable

NR = Not Recommended

Figure 2.2: Compatibility of non-metallic materials with gasses. Adapted from ISO 11114-2

Viewing Glass

When determining which viewing glass to use, the three main design drivers were strength, temperature, and chemical resistance. Many commercial sight glasses are

made of Borosilicate glass because of its low cost, functional operation at standard temperatures, and being inert to most chemicals. However, a comparison with Aluminosilicate glass in Table 2.1 shows Borosilicate glass' weakness. To ensure our project could safely operate at the temperatures we wanted and potentially higher in the future, Aluminosilicate glass was chosen.

Table 2.1: Aluminosilicate Glass vs. Borosilicate Glass

Material Properties	Aluminosilicate Glass	Borosilicate Glass
Density	2.63 kg/m^3	2.23 kg/m^3
Young's Modulus	81 GPa	64 GPa
Thermal shock resistance	300 $^\circ C$	160 $^\circ C$
Working temperature	660 $^\circ C$	230 $^\circ C$

2.2.3 Sensors and Components

Before a final design of the pressure vessel could be made, all sensors and components which would interact with the vessel had to be selected. When choosing all items that would be in contact with the vessel special consideration had to be taken for the pressure and temperature requirements.

Mixer

The component which took priority due to its form factor and difficulty to acquire was the mixer. To ensure its compatibility with our system and smooth operation, emphasis was placed on acquiring a model which was hermetically sealed and contained an electromagnetic clutch . Ultimately, the Cyclone 075 mixer, seen in

Fig. 2.3, was chosen due to its ability to operate at high pressures and temperatures. Its M36x1.5 threaded connection with gasket is rated for 160 Bar, which is above the system requirements. The mixer was equipped with the optional ceramic ball bearings to reduce the unwanted vibrations of the shaft during operation.

Figure 2.3: Buchiglasuster cyclone 75 mixer

Temperature Sensor

The temperature sensor was deliberately chosen after the mixer to ensure there were no clearance issues with the mixer shaft and impeller. Having the internal volume set, there were three main criteria which dictated the form factor of the temperature sensor. First, the sensor needed to have a 1/4" National Pipe Thread (NPT) connection to withstand the working pressure. Second, the insertion length of the probe needed to be less than 30mm to ensure it would fit in the vessel. Lastly, it needed to be hermetically sealed, submersible, and corrosion resistant to withstand the environment of the thermostatic bath. Fig. 2.4 shows the chosen PT-100 Ω resistive temperature sensor from WIKA [model TR33-Z-P2]. All additional wires and components for data collection were also acquired from WIKA.

Figure 2.4: PT-100 Ω resistive temperature sensor from WIKA

Pressure Sensor

To accurately record pressure data for the production of a miscibility plot, a pressure transducer is required. The pressure transducer was not required to be submersible like the temperature sensor, but it still needed to operate within the vessels set temperature and pressure range.

Due to market shortages, a pressure sensor able to handle 160 °C was not readily available. To address this issue, a cooling element, seen in Fig. 2.5, was acquired to work in conjunction with the pressure transducer to avoid critical failure and allow for data acquisition over the desired temperature ranges. The pressure transducer also needed a data logger and USB interface to record and display data in real time on the computer. All required software was provided by the manufacturer

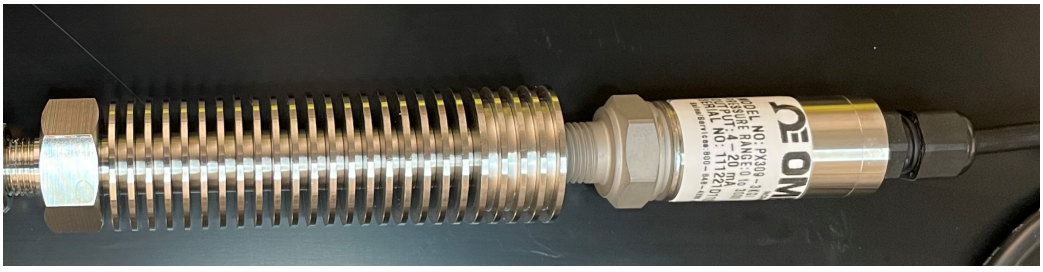

Figure 2.5: Pressure transducer and cooling element from Omega

2.2.4 Design Iterations

Initial Concept

At the beginning of the engineering design process, there are numerous potential configurations which can give rise to a product which meets the needs of a project. Rarely is it possible to envision the single best product design from the outset. Each different design will come with its own strengths and weaknesses; it is only by comparing alternative designs and making sure to prioritize the original requirements that a final concept can be formed [11].

Since there were no commercially available pressure vessels to meet our needs, it was necessary to design it in-house. The goal of the initial draft was to visualize how the pressure vessel needed to be designed to meet the aforementioned criteria. While an ideal pressure vessel would be spherical to evenly distribute the internal stresses, spherical pressure vessels are extremely difficult to manufacture due to their inherent inability to withstand manufacturing defects. A round vessel would also require specially designed sight glasses and a large amount of welding to allow for additional ports. Another option was a purely cylindrical vessel, which has been used in miscibility testing, but this shape would introduce increased manufacturing complexity due to the need for welding to create necessary ports [30]. A cylindrical vessel would also need the design of a support system to prevent unwanted movement induced by the mixer. Inspiration for the first draft was drawn from high pressure sight glasses which have rectangular bodies with cylindrical cross sections. Fig. 2.6 shows the initial concept of a rectangular pressure vessel

with cylindrical internal cross section. This rectangular form factor would allow for a simpler machining process, with the main housing being machined out of a solid block. Alongside ease of manufacturing, this design would be the most forgiving of imperfections introduced during manufacturing. It's ability to stand upright would also eliminate the need for an external support system.

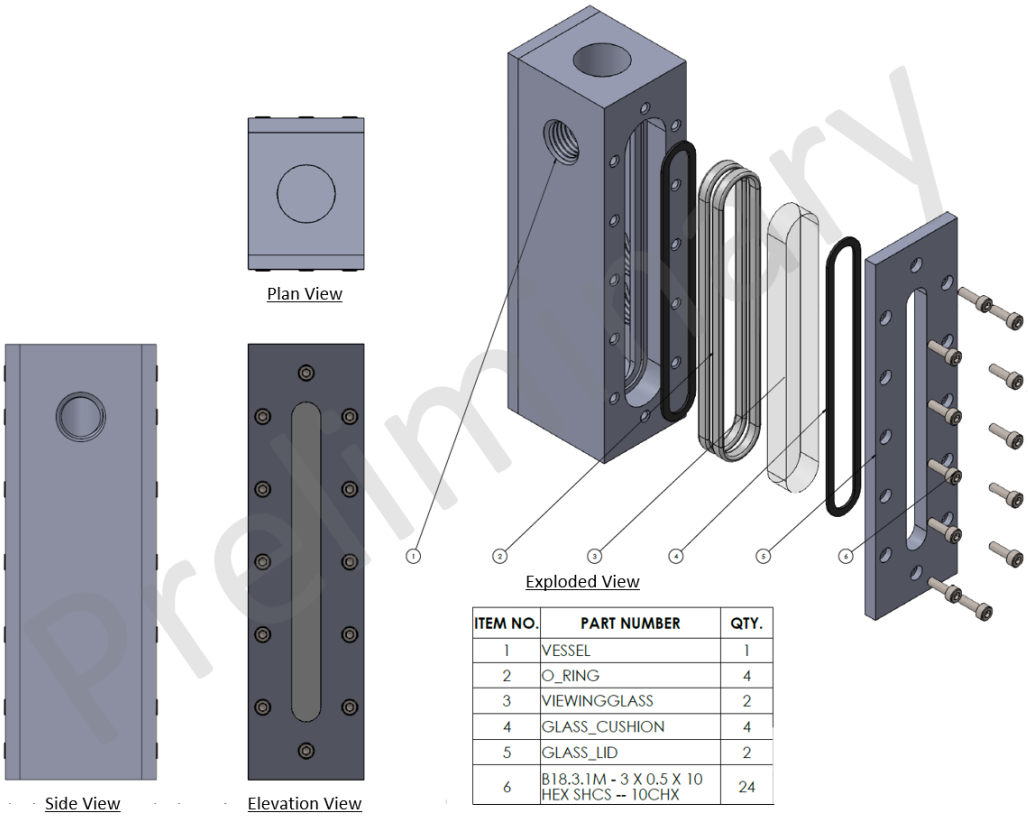

Figure 2.6: Prelimary drawing of first vessel iteration modeled on Solidworks

This initial concept consisted of the vessel body, o-rings, viewing glass, glass cushions, glass lid, and hex bolts. The vessel body had four threaded ports. The first port on the top of the vessel was included to allow for the attachment of the

mixer. At this point, the final mixer had not been selected so the diameter of this port was merely for preliminary design purposes. Ports two and three on the right side of the vessel were intended as connection points for the temperature and pressure transducers. The final port on the top left hand side was earmarked as the charge port for the refrigerant and lubricant.

To visually inspect the lubricant and refrigerant mixture during testing, it was necessary two have sight glasses on both ends of the pressure vessel to allow sufficient light to shine through. The sight glass was designed to be compressed between the gaskets and and fit inside the glass cushions to reduce movement and dampen vibrations.

Second Iteration

Once the initial concept had been created and it seemed plausible to manufacture, the next step was to identify final port sizing. The largest item which had the greatest impact on vessel size was the mixer. The mixer had a M36x1.5 threaded connection which dictated the size of the top port of the vessel. Attached to the main housing of the mixer was a stirrer shaft and impeller. For the 32mm diameter tri-blade impeller attached to the mixing shaft to rotate freely, the internal diameter of the cell needed to be 34mm. The additional 2mm of clearance was necessary to account for manufacturing tolerances and vibrations induced by the rapid spinning of the shaft. Given this internal diameter, it was now possible to calculate the necessary minimum wall thickness for the vessel based on the BPVC Section VIII Division 2 equation 4.3.1 (eqn 2.1). Where inner diameter of the vessel, D = 34mm.

Internal pressure, P = 150 bar. Maximum allowable stress, S = 10,200 psi. Joint efficiency, E = 1. The resultant minimum wall thickness was calculated to be t = 5.4mm

$$t = \frac{D}{2}(exp[\frac{P}{S}] - 1) \tag{2.1}$$

Next, the size and placement of the bolts needed to be calculated. To determine an initial estimate for the bolt sizing, the procedure proposed by the Verein Deitscher Ingenieure (VDI) 2230 was followed. Eqn. 2.2-2.3 were used to determine the approximate axial and transverse forces with gage pressure (p_g) = 150 bar, inner diameter (d_i) = 34mm, design factor (n_d) = 4, mass of the face plate (m_c) = 1.3 kg, and number of bolts (n) = 12.

$$F_{axial} = \frac{n_d p_g \pi d_i^2}{4n} \tag{2.2}$$

$$F_{transverse} = \frac{n_d m_c g}{n} \tag{2.3}$$

Referencing VDI 2230 Part 1, with values for F_{axial} = 4500 N, $F_{transverse}$ = 4 N, and assuming minimum coefficient of friction between clamped parts for steel to be .1 [VDI 2230 Part-1 page 114] a M10 bolt size was chosen.

With the necessary bolt size, it was possible to determine the placement of the bolts required by industry standards. Since the face-plates of the vessel are rectangular and not the typical circular design found in BPVC Section VIII Division 1 or 2, additional standards needed to be referenced to ensure proper design. In this case, British Standards Institutions (BSI) Published Documents (PD) 5500, Enquiry Case 5500/133 was consulted to produce initial design calculations because

it provides guidance for rectangular designs. Eqn. 2.4, found in BSI PD Enquiry Case 5500/133 section 2.3.6, was calculated with an initial bolt diameter (d_b) = 10 mm, gasket factor (m) = 3, Young's Modulus (E) = 190000 MPa, and face plate thickness = 10 mm. With these parameters the maximum spacing between centers of the bolts on the long and short sides (P_{bmax}) was calculated to be 36.9 mm. Since the height of the face-plate would be 152mm, a total of five bolts were needed per side of the viewing glass cut out and additional bolts were needed above and bellow the cut out.

$$P_{bmax} = \frac{t(6[\frac{E}{200000}]^{.25})}{m+.5} + 2d_b \tag{2.4}$$

Now that a vessel with finite dimensions was designed, an in house 3D printer was used to produce an initial prototype out of ABS plastic. The purpose of this prototype , seen in Fig. 2.7, was to test the port sizing with the available equipment. If any issue arose during this process, the design would be adjusted as needed before being sent for actual manufacturing. All available equipment was attached and no issues arose.

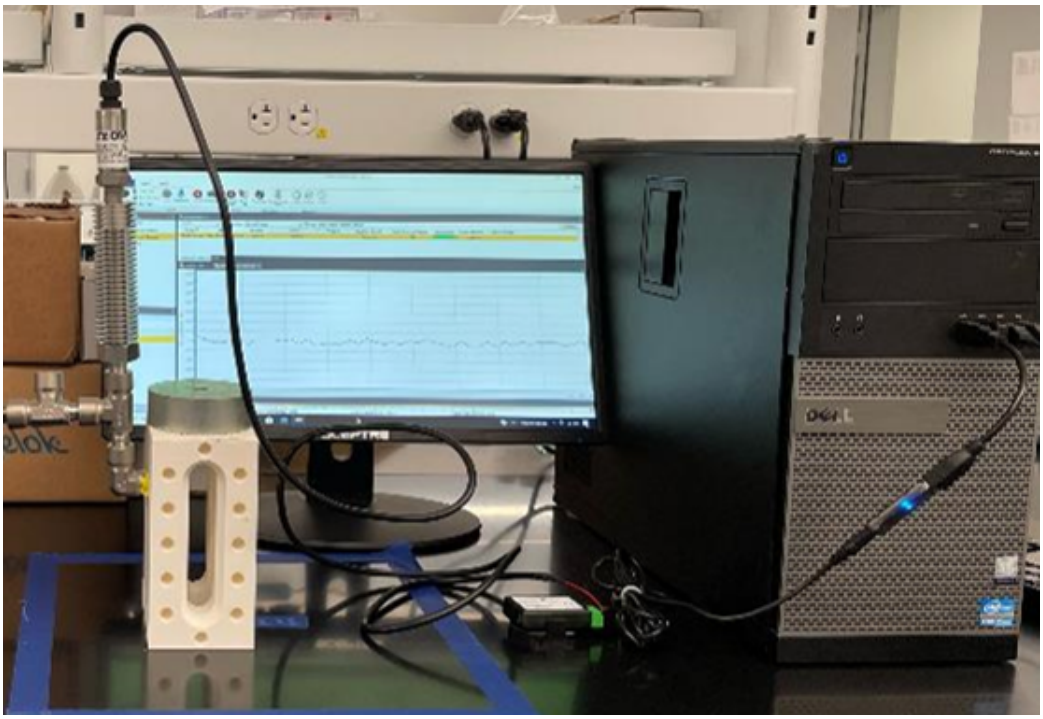

Figure 2.7: Pressure vessel prototype with pressure sensor

Since the vessel will be subject to large internal pressure, it is pertinent to take all possible safety precautions. This includes evaluating the maximum stored energy which could be released in the event of a catastrophic failure. Having this energy value is necessary when determining the appropriate safety system needed to prevent harm. To calculate the stored energy, eqn 2.2 was used. To determine the internal energy the volume of the vessel, absolute pressure, pressure drop if vessel were to burst, and adiabatic exponent of refrigerant were needed. The internal volume of the vessel is 102 ml and will remain constant through all testing since it is geometrically bound. The pressure drop if the vessel were to burst would be 1 ATM since we are near sea level. The absolute pressure of the vessel is test

dependent, but the maximum allowable working pressure (MAWP) will be used for safety precautions. This will occur when using compressed CO2 at 150 bar (2100 psi). The adiabatic exponent is also test dependent since it is a ratio of specific heats. The value for carbon dioxide is variable but is generally close to 1.3. Given this specific test scenario, the stored energy is roughly 4.5 KJ. For reference, 1 gram of TNT contains roughly 4.62 KJ of energy.

$$W = (\frac{P_1 V_1}{K-1})[1-(\frac{P_1}{P_2})^{\frac{(1-K)}{K}}] \tag{2.5}$$

Final Design

In preparation for the manufacturing of the vessel, certain aspects of the vessel had to be adjusted to facilitate the manufacturing process. Although this vessel would not go through the full ASME certification process, it was necessary to at minimum have the vessel undergo a hydrostatic pressure test. This test would subject the vessel to 1.3x the MAWP and the vessel would be checked for leaks and any deformation. Since the pressure of the hydrostatic test is larger than the MAWP, the thickness of the sight glass had to be increased by .5 cm. Although this led to the widening of the vessel by 1 cm, the internal volume remained constant so the energy storage calculation did not need to be redone.

Post Production Modifications

After the manufacturing of the pressure vessel was finished, a few issues arose which needed to be addressed to ensure proper functionality. The first issue was the

threaded connection on the top of the vessel, designated for the mixer, was incorrect for the 160 bar pressure rating. While the manufacturer of the vessel produced the threaded connection to the spec which was provided, due to a clerical error, the wrong spec was provided. The connection which had already been machined, seen on the right of Fig. 2.8, would only be able to withstand pressure up to 60 bar. To fix this issue, an adapter of the correct dimension, seen on the left of Fig. 2.8, was produced and welded to the top of the vessel. The pressure vessel underwent another hydro-static pressure test to ensure its continued structural integrity.

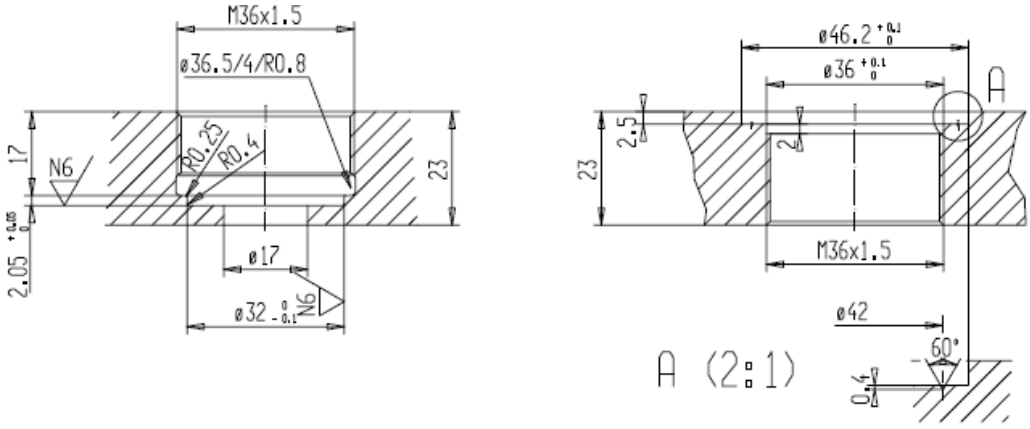

Figure 2.8: Correct connection design [Left] and incorrect connection design [Right]

The second issue which arose was an interference between the mixer and the aforementioned adapter. This adapter had an opening with the diameter of 17mm and the mixer needed a minimum of 18mm to rotate freely. After consulting the manufacturer, the correct diameter for the opening was determined to be 21mm. The hole of the adapter was able to be widened in-house using a Computer Numerical Control (CNC) machine with accuracy of up to 1/10th of a millimeter.

Fig. 2.10 shows a comparison of the original and corrected dimensions. After the adapter opening was increased, there was no longer an interference and the mixer shaft could rotate freely.

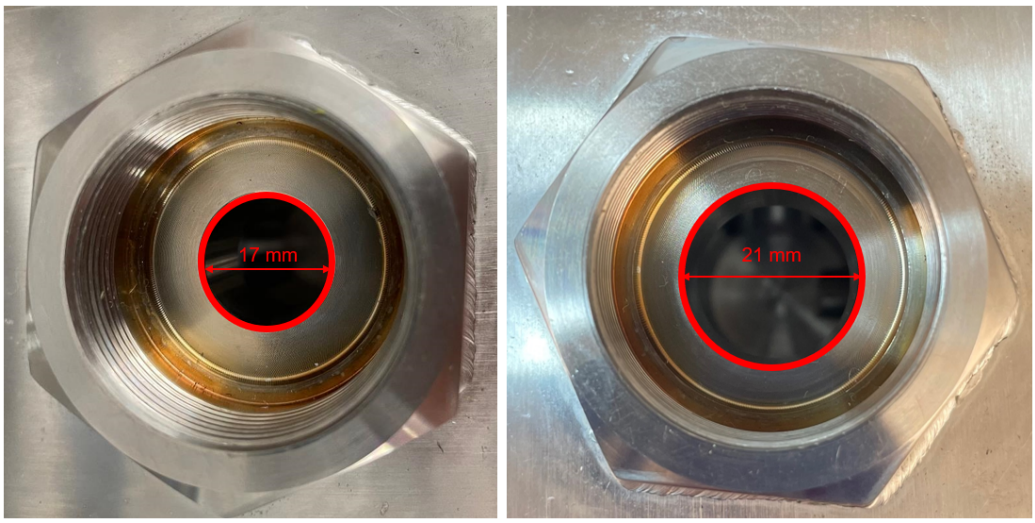

Figure 2.9: Mixing port original diameter [left] and corrected diameter [right]

2.3 Temperature Regulation

2.3.1 Criteria

While the pressure vessel was designed to withstand a wide temperature range, a separate system was needed to get the vessel to accurately reach and sustain those temperatures. According to ASHRAE Guidline 38-2018, the appropriate ways to heat metal pressure vessels include: oven, induction heating, or oil bath. Since our application also called for the cooling of the pressure vessel, it was most convenient to employ a temperature regulating bath.

2.3.2 Components

Figure 2.10: Refrigerated recirculator and bath [red arrows indicated flow direction]

The temperature regulation system in Fig. 2.10 is made up of two main units, the refrigerated recirculator and the external thermostatic bath. The refrigerated recirculator [VWR Catalog No. 89202-978] was modified to allow for an open loop system. 1/4" diameter high pressure chemical hoses were attached to the rear inlet and outlet ports of the recirculator to divert the flow from the main refrigerated recirculator housing into the bath. To reduce system inefficiency, the hoses were insulated with 3/4" thick polyurethane foam with an R value of 3. Additionally, the outlet hose from the recirculator was fitted with a flow adjustment valve. Without a flow control valve, an imbalance in the volumetric flow rate entering and leaving

the recirculator would occur. This flow imbalance leads to fluid starvation of the system, which forces the recirculator to automatically shut down.

The thermostatic bath, where the pressure vessel will remain during testing, consists of a modified 304 SS batch can with a 2" sight glass in the front and rear. The sight glasses were welded onto the bath to allow for visual analysis of the vessel contents during testing. To ensure optimal thermal performance, the bath is insulated with 1 1/4" polystyrene foam with an R value of 5.8.

2.4 Proposed Test Procedure

This proposed test procedure, seen in Fig. 2.11, is for the miscibility testing which aims to acquire data on lubricant-refrigerant mixtures. The first step in preparing to run a test is to flush the system and clean it using iso-propyl alcohol (IPA). Once the system has been cleaned with a flush, then it is necessary to remove the test cell and clean it individually. If there are any components still attached at this stage, they should be removed. To facilitate the cleaning of the inside of the pressure vessel, remove the bolts, viewing glasses, and gaskets. Once again, use IPA to clean all surfaces and crevices of the pressure vessel. After everything has been thoroughly cleaned and dried, it must be reassembled, and bolts re-tightened. After proper cleaning and reassembly, the test cell is ready for use again.

Before charging the lubricants and refrigerants into the test cell, all quantities must be accurately quantified based on the desired mass percentage for the test. To calculate the oil and refrigerant mass percentages, Eqs.2.6-2.8 may be used [31].

$$m_r^v = \rho_r^v V^v \tag{2.6}$$

$$\omega_r = \frac{m_r - m_r^v}{m_r + m_{oil} - m_r^v} \tag{2.7}$$

$$\omega_{oil} = \frac{m_{oil}}{m_r + m_{oil}} \tag{2.8}$$

The volume of the refrigerant oil mixture must also be greater than 70% of the test cell volume to reduce the effects of the vapor volume on the liquid [30]. Charge the refrigerant into the weighable cylinder until the desired mass has been transferred. This step must also be followed with the lubricant. Per ASHRAE Guidline 38-2018, you must first charge the vessel with the desired lubricant before adding the refrigerant. Once the lubricant has been accurately quantified, the test cell will be placed under vacuum to .001 Torr to degas the lubricant. After the lubricant is charged into the vessel, the lubricant vessel must be weighed. This weight is then compared to the initial weight to calculate how much lubricant was transferred into the pressure vessel. If the desired amount of lubricant was charged into the vessel you may proceed, else charge more lubricant until desired amount is reached. The same steps for weighing the refrigerant and charging it must be followed as the lubricant. Once the final values for the mass of the lubricant and refrigerant are obtained, it is possible to calculate the final mass fraction. If the result is inaccurate then whichever constituent needs to be added can be adjusted until the correct mass fraction is achieved.

With the mixture ready, the thermostatic bath will be set to the desired tem-

perature. Monitor the temperature of the bath and vessel. Also keep a close eye on the pressure gauge to make certain the value does not deviate by more than +- 5% during the temperature change. The temperature of the bath will be considered stable when it reaches +- .1 °C of the set temperature. Thermodynamic equilibrium will be reached when the temperature difference between the bath and the vessel is less than 1.5 °C.

Once the thermodynamic equilibrium has been reached, the constituents can be mixed at the desired speed until homogeneous. Temperature, pressure, and visual data will be recorded for 3 minutes after constituents have been mixed and reach thermodynamic equilibrium. This procedure will then be repeated in the desired temperature increments over the desired temperature range until all data has been collected.

2.5 Summary

To ensure proper design of a pressure vessel, all design criteria had to first be clearly and concisely established. The three main design drivers for this vessel were the operating pressure of 150 bar, temperature range from -40 °C to 160 °C, and inclusion of a mixer. Appropriate materials for this vessel were selected based upon fundamental engineering principals and standards. Once the materials and components were chosen, it was possible to begin the designing of the vessel. Industry standard guidelines were followed and SolidWorks was used to aid the design process. Additionally, a system for temperature regulation was created and

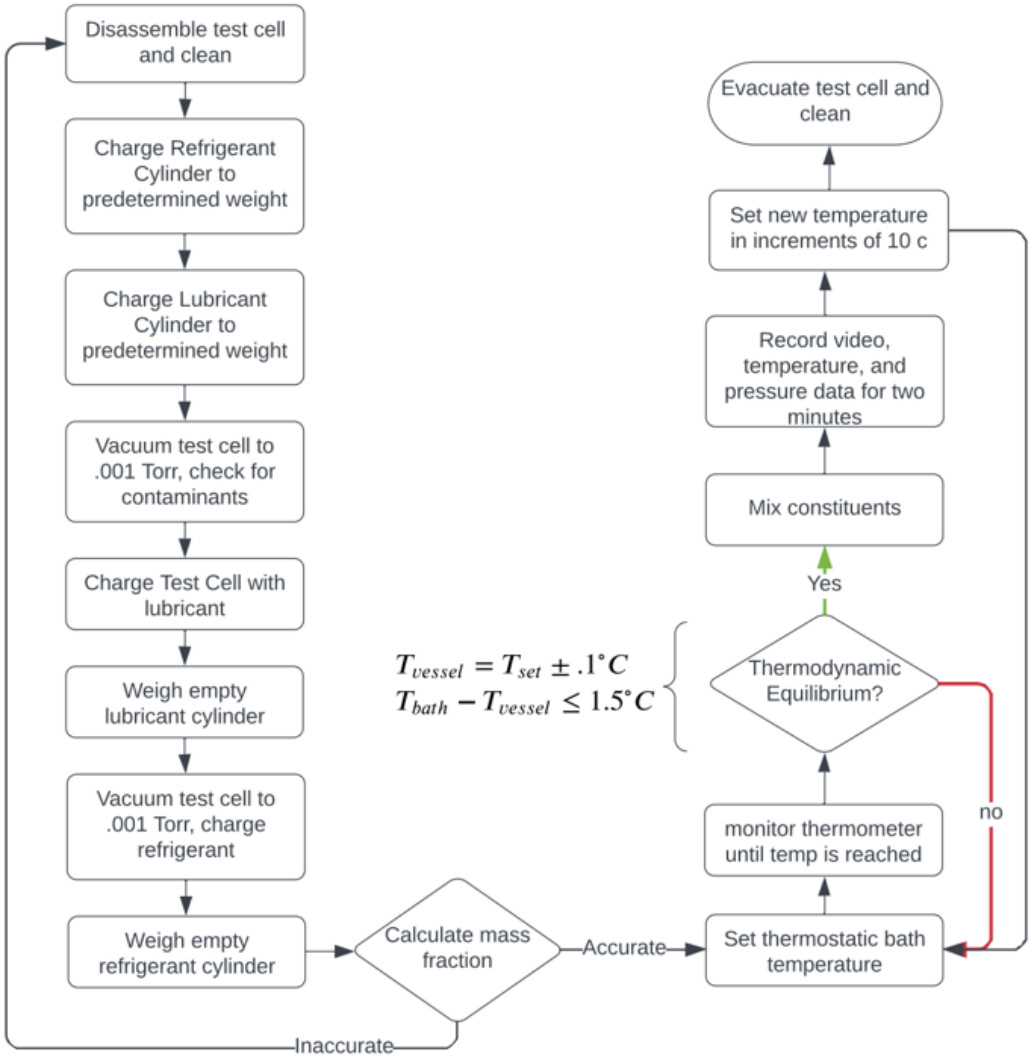

Figure 2.11: Proposed Miscibility Testing Procedure

a testing procedure was proposed.

3. Simulations

3.1 Introduction

In this chapter, the design simulations which helped inform the design solutions in the previous chapter will be discussed. First, stress simulations were conducted on the vessel prototypes to ensure no point of the vessel would undergo drastic deformation. Second, a series of Computation Fluid Dynamics (CFD) simulations were conducted to determine the impeller shape to optimize mixing in the vessel.

3.2 Stress Analysis

All stress analysis were performed with SolidWorks. SolidWorks is a commercial software which is widely used for it's modeling and integrated simulation tools.

3.2.1 Geometry and Mesh

The design of the vessel which was tested can be referenced in the previous chapter.

3.2.2 Boundary and Initial Conditions

The initial conditions for this simulation were determined from the initial design criteria. The internal pressure was set to 150 bar and the test was run at a static temperature of 160 C. To reduce the complexity of the simulation the interface between the faceplate and vessel body was treated as a bonded component under SolidWorks component interactions criteria. A fixed geometry was placed on the bottom of the pressure vessel to avoid movement and allow for the simulation to converge. Although in reality the bottom of the pressure vessel would not be bolted down, this simplification was made because the combined weight of the pressure vessel and attached components would exceed 30lbs.

3.2.3 Results

The results from the simulation, seen in Fig. 3.1, show large areas of stress concentration near the inner edge of the sight-glass ingress and the port locations. These results were to be expected since the inner edge of the sight glass was significantly less reinforced than the main body. Regardless, the maximum stress seen on the vessel was still under the yield limit of 316L SS. The forces on the bolt connections were also analysed to determine if the previously calculated bolt diameter and placement would yield. The resultant axial force seen in Fig. 3.2 , was significantly lower than yield strength of the material, producing a calculated Factor of Safety (FOS) of 6.2. This trend remained consistent for all bolts in the system.

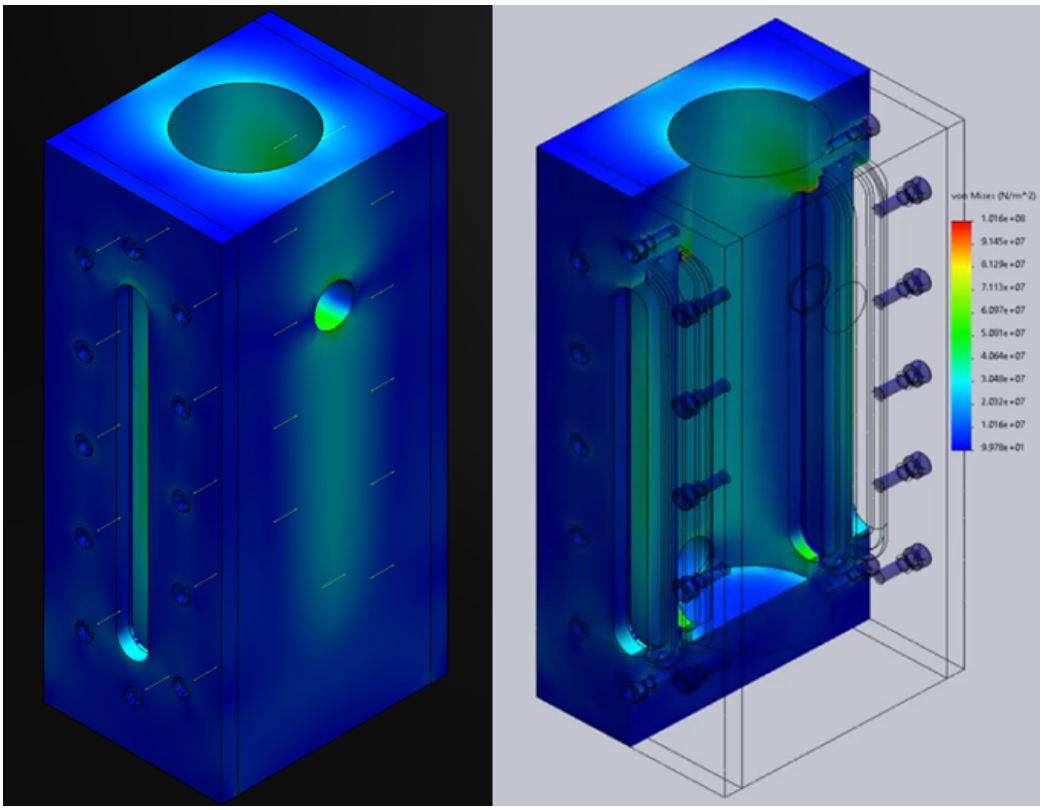

Figure 3.1: Isometric [left] and isometric section [right] view of stress simulation

Type	X-Component	Y-Component	Z-Component	Resultant
Axial Force (N)	0	0	-483.23	483.23
Shear Force (N)	-3.5608	0.79833	0	3.6492
Bending moment (N.m)	-0.0031715	-0.0056466	0	0.0064763

Figure 3.2: Bolt Forces

An additional stress analysis was conducted to determine if changing the vertical position of the lowest port would introduce increased stress in the area. Referencing Fig. 3.3, stress nearest the inside of the vessel changed from nearly 3200 psi, to 3550 psi, and back to 3250 psi for plots a, b, and c respectively. Although there was a slight increase in the localised pressure seen from the inner

side of the moving from position a to b, transition from a to c led to an even smaller change in stress. These results were used to determine that no drastic change would results from repositioning the port 2 cm higher in the vertical direction.

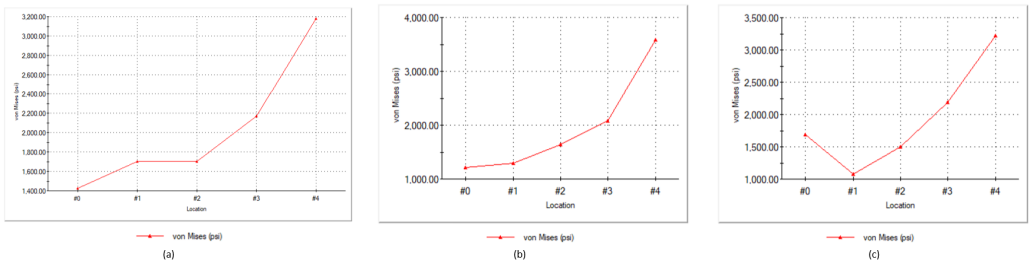

Figure 3.3: Plots of local stress at the bottom surface of the port. Location 0 designates edge closest to vessel outside and Location 4 designates edge closest to vessel interior (a) Original location (b) port moved 1 cm higher than original location (c) port moved 2 cm higher than original location

3.3 Single Fluid Mixing Analysis

In practice, it is difficult to try and physically quantify impeller-induced turbulence; moreover, trying to do so for numerous impellers would be costly and time consuming. To circumvent real world limitations, CFD can be used to analyze the fluid flow patterns in a system caused by impeller agitation. With impeller design being the most important feature for determining a mixers potential success [10], these simulations will allow for a vast array of tank and impeller geometries to be modeled . The performance of these simulations will inform the final decision on which geometry would be best suited for our application. Ensuring properly uniform concentrations of the mixed constituents is paramount for accurate data

collection and needed to ensure efficient and economical use of expensive chemicals [34]. All design and simulations for this section were conducted using the commercially available software, COMSOL Multiphysics.

3.3.1 Geometry and Mesh

The library of COMSOL impellers was used and their dimensions were altered to suit the needs of these simulations. A total of 3 different impellers were used, including a curved Rushton impeller, C-shaped blade, and hydrofoil. These impellers were chosen because they are either sold by our mixer manufacturer or they are commonly cited in literature .[24, 5, 34, 38]. Each test was conducted in a simplified cylindrical cell with a height of 15 cm and radius of 5 cm. These dimensions were chosen to facilitate simulations and allow for easier visualisation of mixing phenomena.

The “Normal” mesh setting in COMSOL was used to produce approximately 322780 elements. Fig. 3.4 and Fig. 3.5 show the visualisation of the created system meshes. COMSOL has an integrated adaptive mesh capabilities to ensure higher resolution at points of interest, closer to the impeller, and lower resolution further away from the intense mixing. By retaining resolution in areas of high importance and reducing resolution in areas of low importance, the simulation will save computational resources while not sacrificing critical accuracy. The adaptive meshing also produces multiple types of meshing elements to increase mesh fidelity, including tetrahedral, quadrilateral, and prism elements. The mesh density was limited by the hardware the simulation was running on.

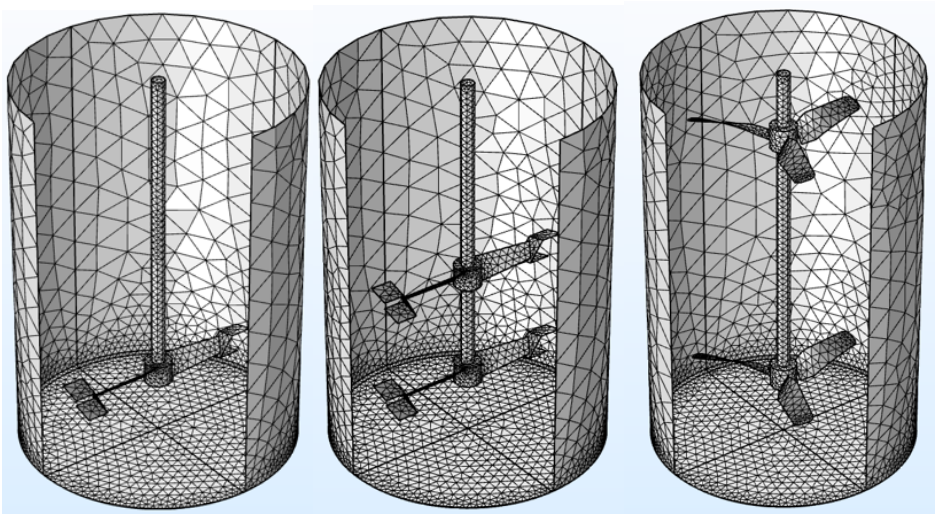

((a)) ((b)) ((c))

Figure 3.4: (a) System mesh with C blade impeller (b) System mesh with stacked C blade impellers (c) System mesh with stacked constant pitch blades

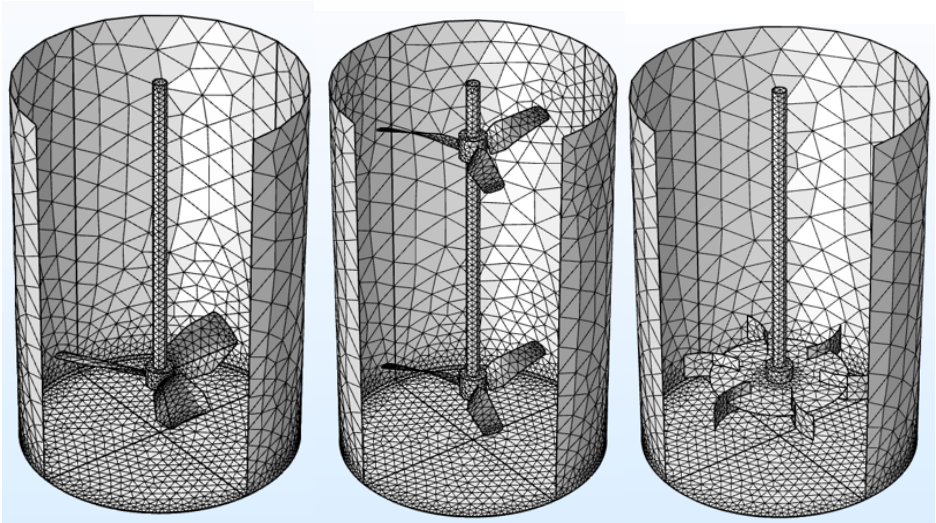

((a)) ((b)) ((c))

Figure 3.5: (a) System mesh with hydrofoil impeller (b) System mesh with stacked hydrofoil impellers (c) System mesh with curved Rushton impeller

3.3.2 Solvers

COMSOL's "Frozen Rotor" study was leveraged which uses centrifugal forces in place of movement, the parts which would typically rotate remain in place, thus reducing the complexity of the calculations. This study can compute the velocity, pressure, turbulence, concentration, and temperature of the fluid in the system. This study is built using the fully coupled Newton's method with Jacobian updates at every time step. The Jacobian updates allow for faster convergence at the cost of computational power.

3.3.3 Results and Discussion

From the COMSOL simulations, plots showing eddy diffusivity and velocity vectors were generated. These plots show the general flow patterns each type of impeller would produce. Eddy diffusivity was chosen as the metric to compare the turbulent fluid dispersion rate of different impellers.

The C shaped blade impeller operate on the principal of producing axial flow in opposite directions which will in turn increase turbulence [34]. In Fig. 3.6, it is observed that there is a great deal of mixing occurring locally near the impeller surfaces. Large Eddys are created right above the c shaped blades which encourage vertical mixing, but the mixing potential is reduced to nearly half of its peak towards the top of the vessel. This would suggest that while the impeller is capable of producing strong flow near its body, it would fail to induce great dispersion throughout the tank.

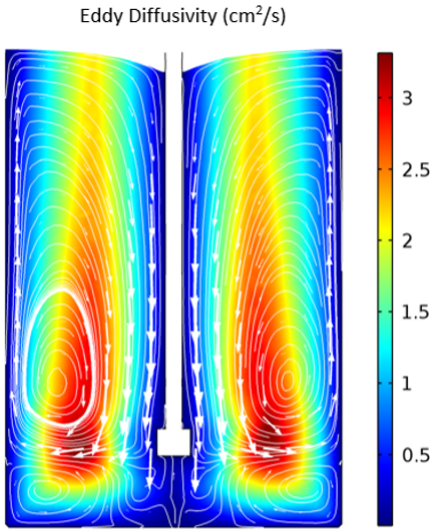

Figure 3.6: Eddy Diffusivity of C shaped impeller blade

To determine if the vertical mixing power of the impeller could be improved, a second c shaped impeller was added. As observed in Fig. 3.7, both the vertical and local diffusivity was improved. The magnitude of the maximum local mixing eddy diffusivity was increased by roughly 50% from nearly 3.3 cm^2/s to nearly 4.5 cm^2/s. Aside from that stark improvement, stacking the c shaped impeller showed a marked increase in vertical mixing potential by nearly 50%.

Remarkably, the curved Rushton impeller was able to produce results which other impellers were only able to approach with stacked configurations. Fig. 3.8 shows strong local mixing around the blades, but more importantly it shows strong vertical mixing throughout the vessel. Out of all the configurations tested, it was able to achieve the highest value for the eddy diffusivity. These results seem to validate the strong mixing trends of this impeller found in other studies [34, 38].

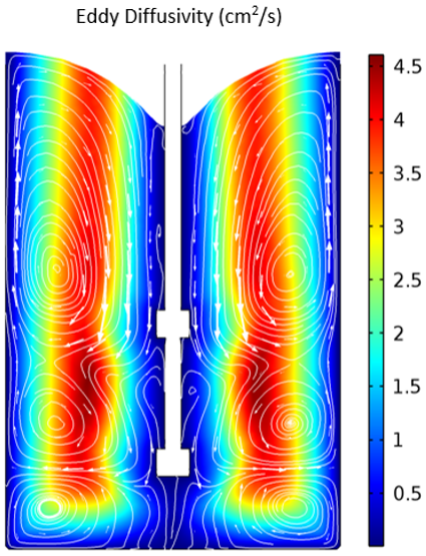

Figure 3.7: Eddy Diffusivity of stacked C shaped impeller blades

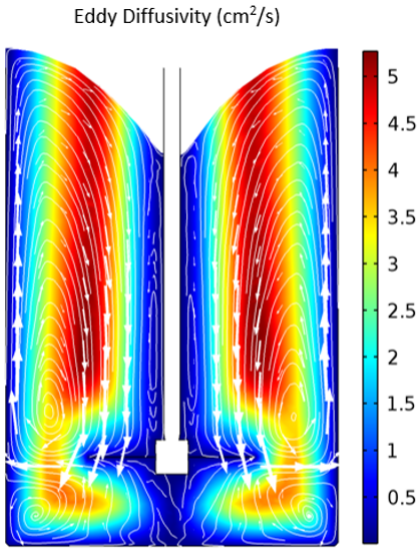

Figure 3.8: Eddy Diffusivity of curved Rushton impeller

Like the other impellers, the Hydrofoil was able to achieve strong eddy diffusivity locally around its blades. However, as seen in Fig. 3.9, the hydrofoil was

also able to achieve strong vertical mixing potential. The overall mixing potential of the hydrofoil was able to remain readily consistent throughout the volume of the vessel, unlike the c shaped blade. Remarkably the hydrofoil was able to produce results similar to that of the stacked c blade impeller and Rushton impeller. This configuration would very well be preferred over a stacked configuration if there are constraints with vertical space.

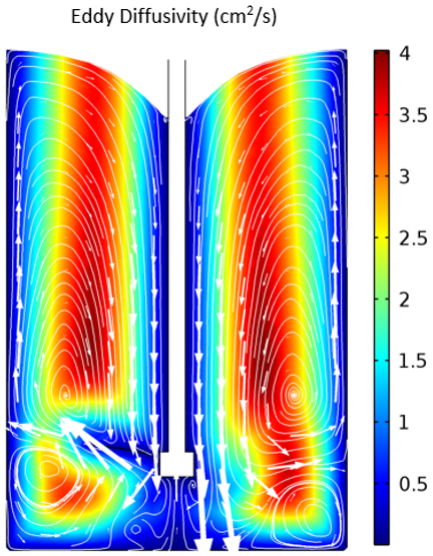

Figure 3.9: Eddy Diffusivity of hydrofoil impeller

The next configuration tested was two hydrofoil impellers positioned on the top and bottom of the vessel. The positioning of this configuration differed from previous examples to analyse if the position of the second impeller changed performance. The second impeller was position 2 cm from the top of the vessel, instead of 4 cm above the initial impeller. While Fig. 3.10 shows a maximum eddy diffusivity value of only 4 cm^2/s, the mixing capability throughout the vessel appears to be

higher on average. This may be due to the impellers being further apart, which gives the flow more time to develop. In Fig. 3.7 we can see the strongest portion of the flow is also between the impellers, but with this new configuration the strong eddy region can be seen throughout the majority of the vessel. Although this configuration does see improved mixing potential throughout the vertical portion of the vessel, the space the second impeller occupies must be weighed against its slim mixing advantages.

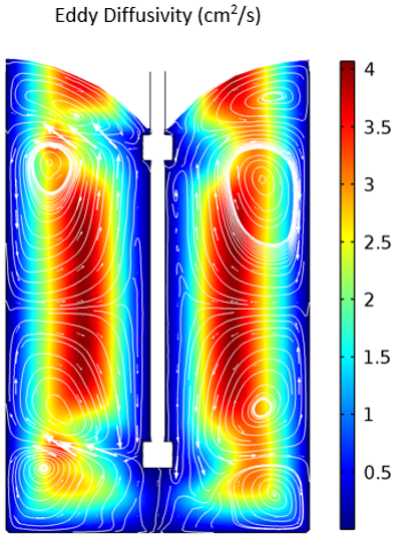

Figure 3.10: Eddy Diffusivity of stacked hydrfoil impeller blades

The final simulations in Fig. 3.11 show the results of having each impeller move in opposite directions. In practice having independently moving impellers would be difficult to obtain. Instead of independent rotation, inverting the impellers would achieve similar effects. Both configurations shows roughly a 10% increase in maximum eddy diffusivity when compared to Fig. 3.10. Surprisingly, the configuration with the best performance had the impeller moving clockwise on top

and counterclockwise on the bottom. This set up showed to have more complete mixing throughout the entire volume of the vessel supported by the large eddy creation near the blades. Further research needs to be done on why this is the case.

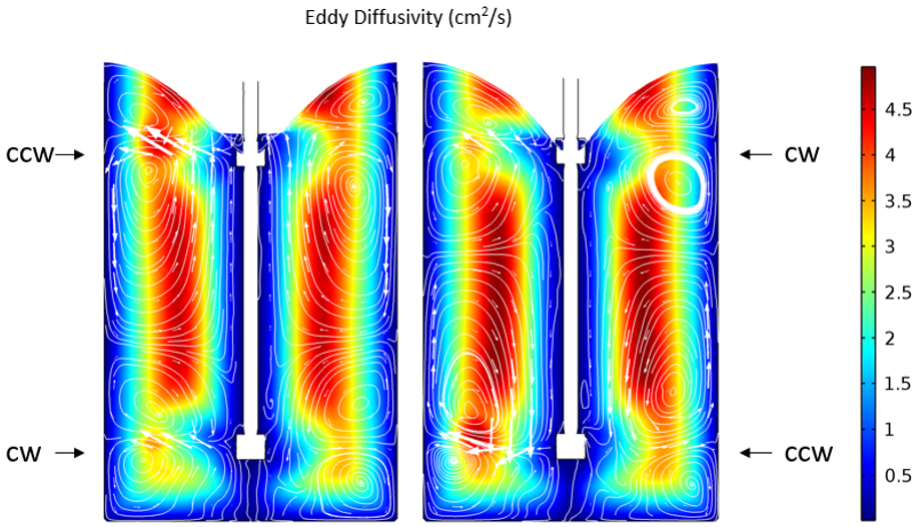

Figure 3.11: Eddy Diffusivity of stacked hydro impellers with alternating rotation

3.4 Multi Fluid Mixing Analysis

3.4.1 Geometry and Mesh

ANSYS internal meshing tool was leveraged to produce the mesh for the impeller and cylindrical body. The mesh of the cylindrical body is broken into the inner and outer domain, seen in Fig. 3.12. The inner domain is comprised of the impeller with shaft and the outer domain contains the tanks walls. Contact boundaries for the fluids were defined in the mesh using ANSYS. The entire model consists

of 61675 nodes and 309145 elements which was limited by the ANSYS student software.

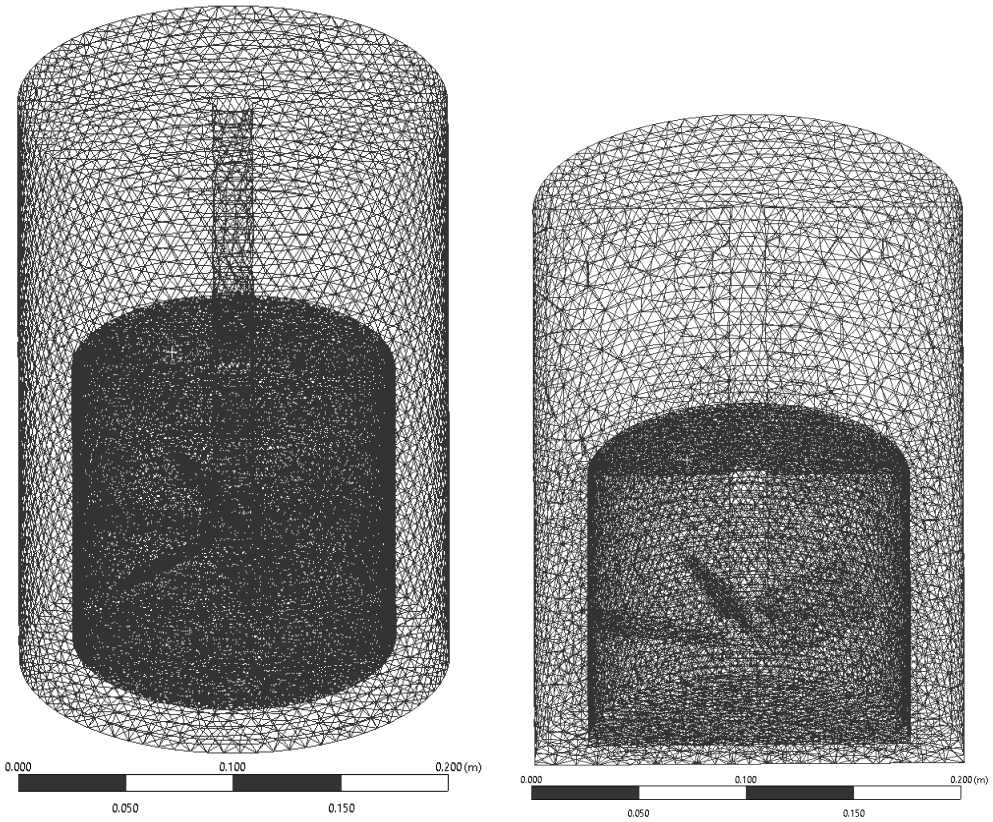

((a)) **((b))**

Figure 3.12: (a) Full system mesh (b) Section view of system mesh

3.4.2 Solvers

The system was solved using a phase coupled SIMPLE algorithm. While this algorithm incorporates phase changes, it operates under the similar principal of the classic SIMPLE algorithm in which the boundary conditions are set, and the

gradients of velocity and pressure are calculated. Then the discretized momentum equation is solved to compute the intermediate velocity field. The mass fluxes are then computed and used to solve the pressure correction equation. This pressure correction equation is then used to update the original pressure field. This corrected pressure field is used to update the boundary pressure corrects, which in turn allows for the correction of the mass fluxes and cell velocities [27]. The phase coupled algorithm differs from the previously described method by coupling via phase and not velocity.

3.4.3 Boundary Conditions and Initial Conditions

The refrigerant properties used in this simulation were for CO2:

$\rho_c = 8.6\ g/cm^3$

$C_p = 3.13\ 10^3 J/KgK$

$\mu_c = 1.37\ 10^{-5} kg/ms$

The properties for the oil in the simulation was for mineral oil:

$\rho_m = .84\ g/cm^3$

$C_p = 3.13\ 10^3 J/KgK$

$\nu_m = 9\ cST\ @\ 40^o C$

These simulations were run with convergence tolerances of 10^{-4} and were solved as if the impeller had a speed of 500 rpm.

3.4.4 Results

The first simulation was solved using the Phase Coupled Simple scheme with First Order Implicit transient formulation. In Fig. 3.13, it is observed that at time 0 the volume fraction of CO2 is roughly equal to 11.3%. Fig. 3.14 shows that as the simulation continues and the agitation of the mixture occurs, the volume fraction seen through the vertical slice that bisects the origin is roughly 9% with higher concentrations orbiting the outside of the inner volume near the impeller. The entirety of this simulation took roughly 25 minutes until convergence.

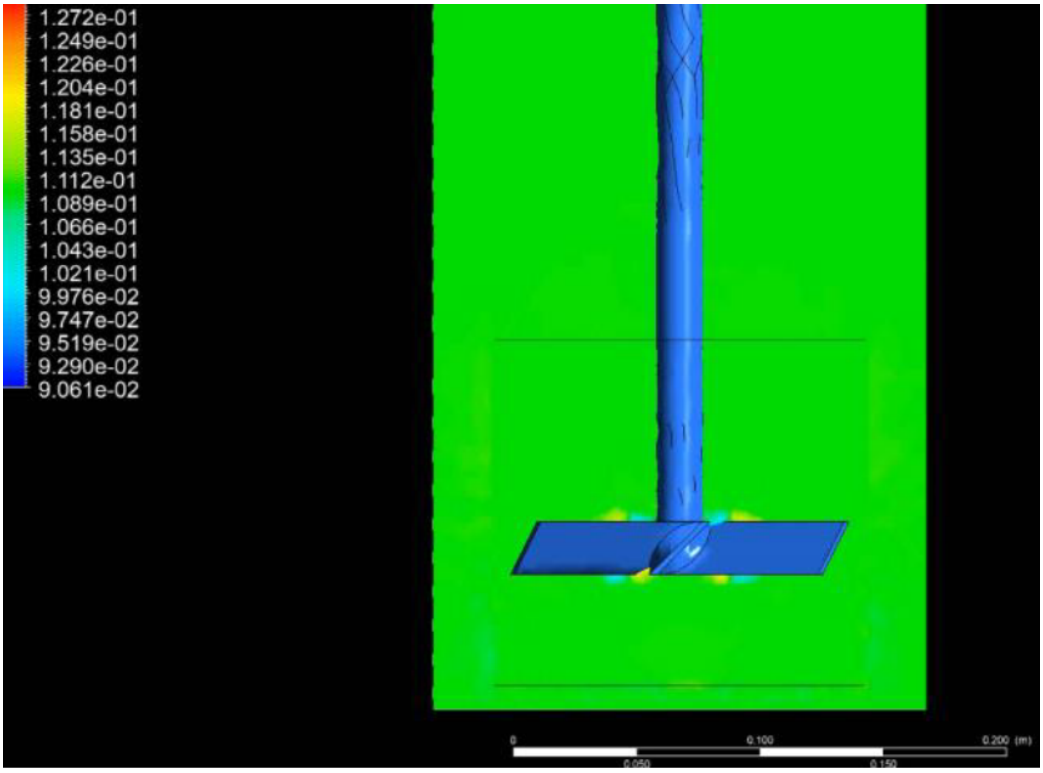

Figure 3.13: ANSYS Simulation: Initial Step

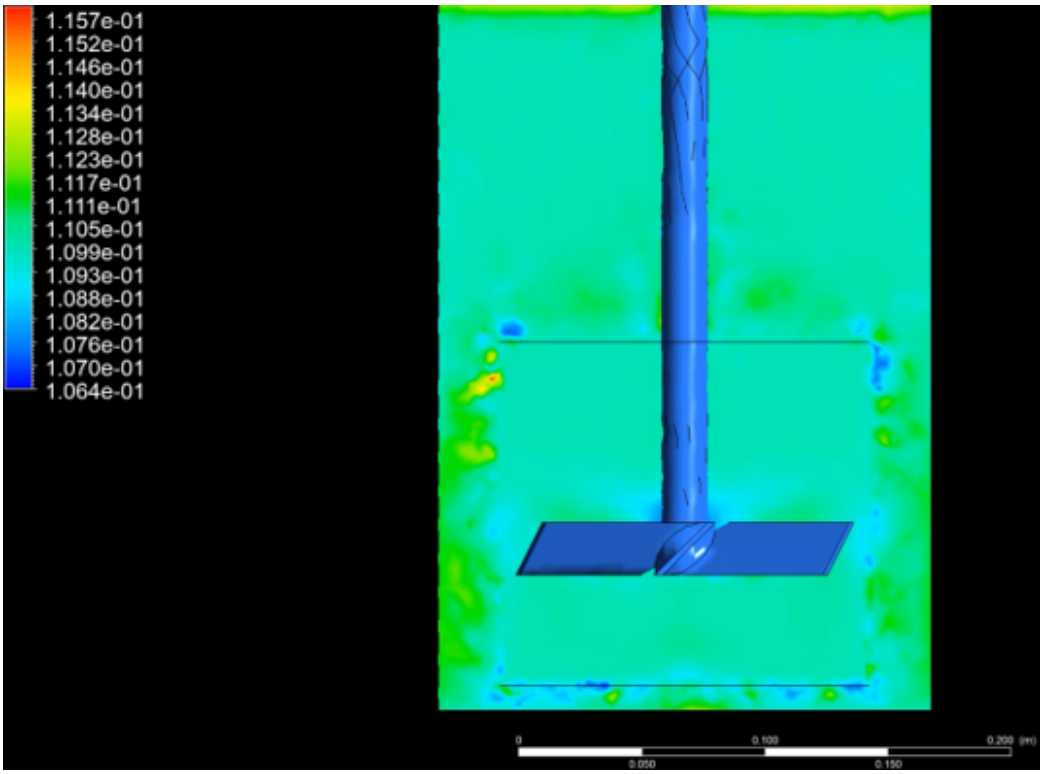

Figure 3.14: ANSYS Simulation: Final Step

The next simulation used a second order implicit formulation. This was done to see if the computational resources needed to run this were worth the potential increase in accuracy. The simulation at time step 0 is equivalent to the first order simulation seen in Fig. 3.13. Fig. 3.15 shows as the simulation continued and finished, the result was roughly 10.9% volume fraction of CO2. This value is too close to the previous simulation to show any significant changes due to a higher order scheme. The time needed for this simulation to reach convergence was roughly 30 minutes, which represents a 20% increase in computational time.

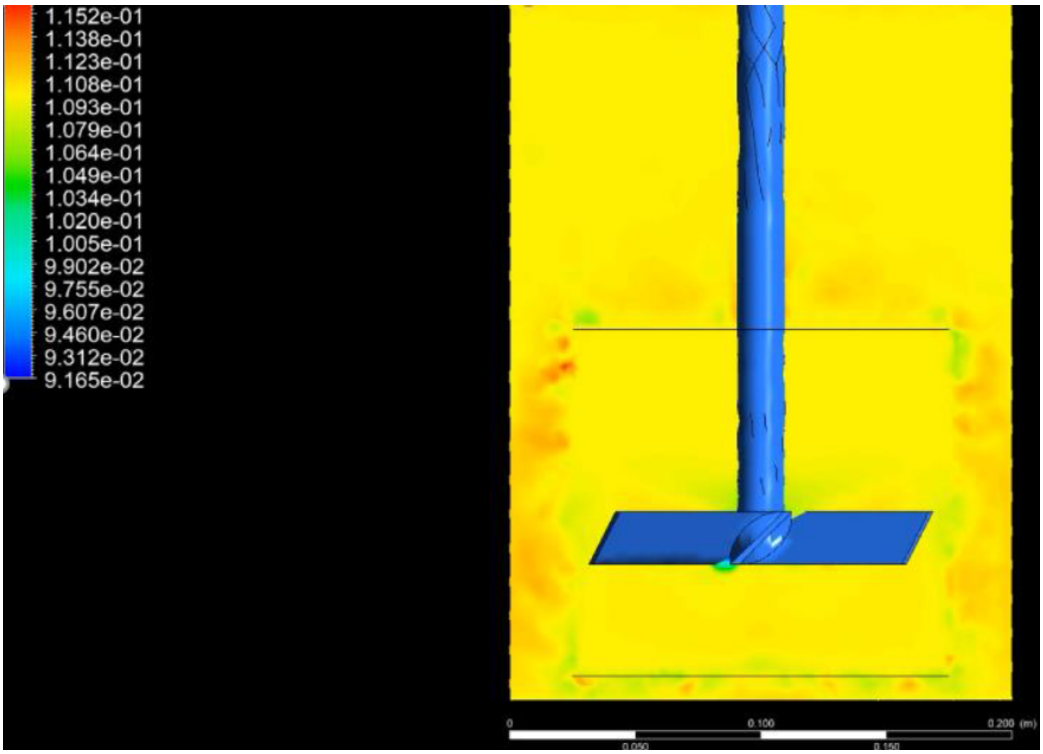

Figure 3.15: ANSYS Second Order Simulation: Final Step

3.5 Discussion

While these simulations showed how CO2 volume fraction changes over time, it would be prudent to see if this trend occurs with other mixtures at similar rates or if it is dependent on viscosity. In tandem, it would be interesting to see how an increase in the pressure of the system would change the results.

When analysing the second order simulation, the negligible change is accuracy was not worth the increased computation time in this case. It is to be noted that the mesh density remained constant from the first and second order simulations.

Increased mesh density is likely needed to see a major change in accuracy.

3.6 Summary

Both COMSOL Multiphysics and ANSYS can be leveraged to analyze fluid mixing for future research purposes, specifically for lubricant-refrigerant mixtures intended for use in compressors. The phase coupled SIMPLE scheme worked well with this simulation, but analysis for the use of other schemes for high pressure situations need to be explored.

The results of the single fluid mixing analysis provided insight into the flow patterns of the different impellers. The c shaped impeller fared the worst out of all the models, even being outclassed in its dual impeller configuration. These simulations have shown that the rushton impeller has the potential to be the optimal shape for our vessel.

To increase the vorticity and mixing capabilities, either baffles or an extra rotors may be added. Baffles function by establishing axial flow patterns and minimizing the tangential and swirling components of the mixing. Although a second rotor could be added to facilitate mixing toward the top of the vessel, as demonstrated in the single fluid mixing simulations, this design wouldn't be practical in actual application due to space constraints.

4. Conclusion

As the landscape of the refrigeration industry continues to shift, there will be a growing need for miscibility data of refrigerants and lubricants. Without this data, optimal refrigeration systems cannot be designed. This research focused on the design and construction of a pressure vessel to obtain said miscibility data. The design process was guided by current industry standards, found in BPVC Section Viii, and simulations were used to inform final design characteristics. All design problems and issues were tackled with fundamental engineering principals. This research allowed for the production of a pressure vessel that was certified to withstand the designed pressure. Additionally, a system for the temperature regulation of the vessel was designed and deployed. Overall, the completion of this project has laid the ground work and produced the necessary equipment for future miscibility testing.

4.1 Future Work

While expanded PTFE gaskets were chosen due to their robust chemical resistance and high pressure compatibility, there is still further investigation needed into the longevity of the gaskets. As mention previously, the lack of set bolt torque may result in uneven wear on the PTFE gaskets leading to uneven and premature degradation. It has previously been noted that when PTFE gaskets are used in bolted fanged connections and subject to a compressive stress, the PTFE continues to deform over time [7]. This leads to the need for re-torquing of the gasket after 24-hours to ensure the bolts and gaskets maintain the designated stress [35]. Accomplishing this re-torque will only be possible once a set toque is established. Although a set torque for the bolts on the face plate was not established by the manufacturer, further investigation is needed to identify the optimal bolt torque for this system.

Additionally, it is recommended a study be conducted to determine the potential effects of the cooling neck attachment on the readings from the pressure sensor. Depending on the refrigerant and lubricants present, it is a possibility for a phase change to occur in the cooling neck resulting in a change in pressure. While this is speculative and scope of the issue is uncertain, further analysis should be conducted for the specific refrigerants to be used in the future.

Lastly, as discussed in the simulations section, there are different impeller shapes which may effect the mixing potential of the system. Due to time constraints, the Rushton and hydrofoil impellers were not able to be acquired. These impellers

may be produced using in-house metal additive manufacturing and tested in the system.

Bibliography

[1] Abou-Jaoude. “Limits on the use of freons”. In: *Bull. Tech. Bur. Veritas* (Mar. 1993).

[2] C Aprea, R Mastrullo, and C Renno. “Determination of the compressor optimal working conditions”. In: *Appl. Therm. Eng.* 29.10 (July 2009), pp. 1991–1997.

[3] Master Bilt. *Refrigeration U: The Basic Refrigeration Cycle*. en. https://master-bilt.com/general-information/news/refrigeration-u-the-basic-refrigeration-cycle/. Accessed: 2022-7-31. July 2021.

[4] B O Bolaji and Z Huan. “Ozone depletion and global warming: Case for the use of natural refrigerant – a review”. In: *Renewable Sustainable Energy Rev.* 18 (Feb. 2013), pp. 49–54.

[5] J M Bujalski et al. “The Influence of the Addition Position of a Tracer on CFD Simulated Mixing Times in a Vessel Agitated by a Rushton Turbine”. In: *Chem. Eng. Res. Des.* 80.8 (Nov. 2002), pp. 824–831.

[6] Yubo Chen et al. “Experimental study on the contribution of R161 and R1234yf to the miscibility of R32 with lubricating oils”. In: *Appl. Therm. Eng.* 175 (July 2020), p. 115338.

[7] Mandi M Clarke, Kenneth R Grant, and A Fitzgerald (jerry) Waterland. “Initial Investigation on the Effect of Bolt Loading Rate on the Need to Re-Torque PTFE Gaskets in Bolted Flanged Connections”. In: *ASME 2015 Pressure Vessels and Piping Conference*. American Society of Mechanical Engineers Digital Collection, Nov. 2015.

[8] M Fatouh and M El Kafafy. “Assessment of propane/commercial butane mixtures as possible alternatives to R134a in domestic refrigerators”. In: *Energy Convers. Manage.* 47.15 (Sept. 2006), pp. 2644–2658.

[9] L Fusaro. *Preventing Spacecraft Failures Due to Tribological Problems*. https://ntrs.nasa.gov/api/citations/20010049424/downloads/20010049424.pdf. Accessed: 2022-8-1.

[10] Chun-Yan Ge et al. "CFD simulation and PIV measurement of the flow field generated by modified pitched blade turbine impellers". In: *Chem. Eng. Res. Des.* 92.6 (June 2014), pp. 1027–1036.

[11] Dani George, Rahul Renu, and Gregory Mocko. "Concept Generation Through Morphological and Options Matrices". In: *ICoRD'13*. Springer India, 2013, pp. 199–210.

[12] Eric Granryd. "Hydrocarbons as refrigerants — an overview". In: *Int. J. Refrig* 24.1 (Jan. 2001), pp. 15–24.

[13] Don W Green and Marylee Z Southard. *Perry's chemical engineers' handbook*. McGraw-Hill Education, 2019.

[14] Seiichro Hironaka. "Boundary Lubrication and Lubricants". In: (July 1984).

[15] James Huang and Walter Lee. "Sealing and mechanical behaviors of expanded PTFE gasket sheets characterized by PVRC room temperature tightness tests". In: *Mater. Chem. Phys.* 68.1 (Feb. 2001), pp. 180–196.

[16] Yunho Hwang, Jun-Pyo Lee, and Reinhard Radermacher. "Oil distribution in a transcritical CO2 air-conditioning system". In: *Appl. Therm. Eng.* 27.14 (Oct. 2007), pp. 2618–2625.

[17] ISO. *ISO 11114-2*. https://www.iso.org/obp/ui/. Accessed: 2022-8-1.

[18] Xiucan Jia et al. "Phase equilibrium of R1234yf and R1234ze(E) with POE lubricant and thermodynamic performance on the evaporator". In: *Fluid Phase Equilib.* 514 (June 2020), p. 112562.

[19] Mazyar Karampour and Samer Sawalha. "State-of-the-art integrated CO2 refrigeration system for supermarkets: A comparative analysis". In: *Int. J. Refrig* 86 (Feb. 2018), pp. 239–257.

[20] Joseph Karnaz. "Evaluating Lubricants For Lower GWP Refrigerant Compressor Operations". In: International Compressor Engineering Conference (2016).

[21] P S Korinko and S H Malene. "Considerations for the weldability of types 304L and 316L stainless steel". In: *Practical Failure Analysis* 1.4 (Aug. 2001), pp. 61–68.

[22] Lei Liu et al. “Enhanced mechanical durability of perfluorosulfonic acid proton-exchange membrane based on a double-layer ePTFE reinforcement strategy”. In: *Int. J. Hydrogen Energy* (July 2022).

[23] R M Mortier, S T Orszulik, and M F Fox. *Chemistry and Technology of Lubricants*. Springer Netherlands, 2010.

[24] Adnan Ghulam Mustafa, Mohd Fadhil Majnis, and Nor Azyati Abdul Muttalib. “CFD Study on Impeller Effect on Mixing in Miniature Stirred Tank Reactor”. en. In: *CFD Lett.* 12.10 (Nov. 2020), pp. 15–26.

[25] Kashif Nawaz and Moonis R Ally. “Options for low-global-warming-potential and natural refrigerants Part 2: Performance of refrigerants and systemic irreversibilities”. In: *Int. J. Refrig* 106 (Oct. 2019), pp. 213–224.

[26] Petter Nekså. “CO2 heat pump systems”. In: *Int. J. Refrig* 25.4 (June 2002), pp. 421–427.

[27] N R Olsen. *CFD algorithms for hydraulic engineering*. https://folk.ntnu.no/nilsol/cfd/cfdalgo.pdf. Accessed: 2022-8-1. 2000.

[28] Andy Pearson. “Refrigeration with ammonia”. In: *Int. J. Refrig* 31.4 (June 2008), pp. 545–551.

[29] Leslie R Rudnick. *Synthetics, mineral oils, and bio-based lubricants: Chemistry and technology, third edition*. Ed. by Leslie R Rudnick. CRC Press, Jan. 2020.

[30] Arslan Saleem and Man-Hoe Kim. “Miscibility analysis of polyol-ester based oil SW32 with R404A and low-GWP refrigerant R452A”. In: *Int. J. Refrig* 129 (Sept. 2021), pp. 22–31.

[31] Arslan Saleem, Du-Yu Shi, and Man-Hoe Kim. “Experimental investigation of refrigerant R-452A miscibility with synthetic oil SW32”. In: (Apr. 2019), pp. 121–123.

[32] Hans O Spauschus. “Compatibility requirements for CFC alternatives”. In: *Int. J. Refrig* 13.2 (Mar. 1990), pp. 73–78.

[33] N Stosic. “On heat transfer in screw compressors”. In: *Int. J. Heat Fluid Flow* 51 (Feb. 2015), pp. 285–297.

[34] Ian Torotwa and Changying Ji. “A Study of the Mixing Performance of Different Impeller Designs in Stirred Vessels Using Computational Fluid Dynamics”. en. In: *Des. Codes Cryptogr.* 2.1 (Mar. 2018), p. 10.

[35] Alfred F Waterland and James E B Frew. “Determination of Optimum Ambient Temperature Re-Torque Dwell Period for PTFE Based Gaskets”. In: *ASME 2006 Pressure Vessels and Piping/ICPVT-11 Conference*. American Society of Mechanical Engineers Digital Collection, July 2008, pp. 93–101.

[36] Saurabh Yadav, Jie Liu, and Sung Chul Kim. “A comprehensive study on 21st-century refrigerants - R290 and R1234yf: A review”. In: *Int. J. Heat Mass Transf.* 182 (Jan. 2022), p. 121947.

[37] Talha Bin Yaqub et al. “Molybdenum diselenide coatings as universal dry lubricants for terrestrial and aerospace applications”. In: *Mater. Lett.* 275 (Sept. 2020), p. 128035.

[38] R Zadghaffari, J S Moghaddas, and J Revstedt. “A mixing study in a double-Rushton stirred tank”. In: *Comput. Chem. Eng.* 33.7 (July 2009), pp. 1240–1246.

[39] Rui Zhai et al. “Research on miscibility performances of refrigerants with mineral lubricating oils”. In: *Appl. Therm. Eng.* 159 (Aug. 2019), p. 113811.

[40] Vitaly Zhelezny et al. “Prediction of the surface tension for refrigerants and refrigerant-oil solutions (ROS)”. In: *Int. J. Refrig* 40 (Apr. 2014), pp. 241–245.